View metadata, citation and similar papers at core.ac.uk

brought to you by CORE

provided by Elsevier - Publisher Connector

© 2010 BY THE AMERICAN COLLEGE OF CARDIOLOGY FOUNDATION
ISSN 1936-878X/$36.00
PUBLISHED BY ELSEVIER INC.
DOI:10.1016/j.jcmg.2010.08.012

Use of Contrast Enhancement and High-Resolution 3D Black-Blood MRI to Identify Inflammation in Atherosclerosis

Jin Hur, MD,* Jaeseok Park, PHD,*† Young Jin Kim, MD,* Hye-Jeong Lee, MD,* Hyo Sup Shim, MD,‡ Kyu Ok Choe, MD,* Byoung Wook Choi, MD*

Seoul, South Korea

OBJECTIVES We investigated the contributing factors for plaque enhancement and examined the relationships between regional contrast enhancement and the inflammatory activity of atherosclerotic plaques in an experimental rabbit model using contrast-enhanced high-resolution 3-dimensional (3D) black-blood magnetic resonance imaging (MRI) in comparison with histopathologic analysis.

BACKGROUND Inflammation plays a critical role in plaque initiation, progression, and disruption. As such, inflammation represents an emerging target for the treatment of atherosclerosis. MRI findings suggest that contrast agent–induced signal enhancement is associated with the degree of macrophage infiltration and neovessels that can be detected in plaque.

METHODS Ten atherosclerotic rabbits and 3 normal control rabbits underwent high-resolution 3D contrast-enhanced black-blood MRI. Magnetic resonance images and the corresponding histopathologic sections were divided into 4 quadrants. Plaque composition was analyzed for each quadrant according to histopathologic criteria (percent of lipid-rich, fibrous, macrophage area and microvessel density) and imaging criteria (enhancement ratio [ER], ER = signal intensity$_{post}$/signal intensity$_{pre}$). Multiple linear regression analysis was performed to determine independent factors for plaque enhancement.

RESULTS A total of 62 noncalcified plaques (n = 248; 156 lipid-rich quadrants and 92 fibrous quadrants) were identified based on histopathologic analysis. Mean ER values were significantly higher in atherosclerotic vessel walls than in normal vessel walls (2.03 ± 0.25 vs. 1.58 ± 0.15; p = 0.017). The mean ER values were significantly higher in lipid-rich quadrants compared with the fibrous quadrants (2.14 ± 0.31 vs. 1.84 ± 0.21; p = 0.001). Mean ER values were significantly higher in macrophage-rich plaques compared with the macrophage-poor plaques (2.21 ± 0.28 vs. 1.81 ± 0.22; p = 0.001). Using multiple regression analysis, macrophage area and microvessel density were associated independently with ER values that reflected plaque enhancement (p < 0.001).

CONCLUSIONS Contrast-enhanced high-resolution 3D black-blood MRI may be an efficient method to detect plaque inflammation. (J Am Coll Cardiol Img 2010;3:1127–35) © 2010 by the American College of Cardiology Foundation

From the *Department of Radiology and Research Institute of Radiological Science, Yonsei University College of Medicine, Seoul, South Korea; †Department of Computational Science and Engineering, Yonsei University College of Medicine, Seoul, South Korea; and the ‡Department of Pathology, Yonsei University College of Medicine, Seoul, South Korea. This work was supported by a grant from the Korea Healthcare Technology R&D Project, Ministry for Health, Welfare & Family Affairs, Republic of Korea (A090358). The authors have reported that they have no relationships to disclose.

Manuscript received June 1, 2010; revised manuscript received August 2, 2010, accepted August 23, 2010.

A number of studies have suggested that the vulnerability or destabilization of atherosclerotic plaques is related directly to plaque composition (1–3). Atherosclerotic plaques, which exhibit large lipid cores, thin fibrous caps, and a preponderance of macrophages, are at the highest risk of rupture (4–8).

See page 1136

Recent reports have shown that an association of inflammatory cells and neovessels in atherosclerosis is a histologic hallmark of high-risk active lesions (7–10). Therefore, plaques with active inflammation may be identifiable by the presence of extensive macrophage accumulation. Magnetic resonance imaging (MRI) findings suggest that contrast agent-induced signal enhancement is associated with the degree of macrophage infiltration and neovessels that can be detected in plaque (9,10).

ABBREVIATIONS AND ACRONYMS

2D = 2-dimensional

3D = 3-dimensional

DCE = dynamic contrast enhanced

ER = enhancement ratio

Gd-DTPA = gadolinium-diethylenetriaminepentaacetic acid

MRI = magnetic resonance imaging

SI = signal intensities

Contrast-enhanced MRI, which uses gadolinium-based extracellular contrast agents for imaging, provides both morphological as well as functional assessment of atherosclerotic plaque formation (9–14). Gadolinium-based agents passively distribute from the intravascular into the extracellular fluid space. Some previous studies have reported effective contrast enhancement of atherosclerotic plaque in human carotid atheroma (11,12), whereas others have reported that gadolinium-diethylenetriaminepentaacetic acid (Gd-DTPA) is a nonspecific contrast agent and that discriminating between normal and atherosclerotic vessel walls was not possible (15–17). Therefore, the underlying mechanism leading to contrast enhancement within the atherosclerotic vessel wall is not fully understood and is controversial in its efficacy.

Two-dimensional (2D) turbo/fast spin-echo pulse sequences with double-inversion black-blood preparation have been used conventionally for imaging atherosclerotic plaque. However, this technique is limited in spatial resolution along the slice-select direction because of radiofrequency constraints and the gradient hardware system, resulting in a substantial amount of partial volume effects, which obscure image details (18,19). To alleviate these problems, a diffusion-prepared 3-dimensional (3D) balanced steady-state free precession may be used as an alternative, but is susceptible to image artifacts in the presence of field inhomogeneity, particularly in high magnetic fields (20). Therefore, we developed a new, contrast-enhanced black-blood single-slab 3D turbo/fast spin-echo pulse sequence to evaluate quantitatively the inflammatory activity of atherosclerotic plaques in an experimental rabbit model. We hypothesized that plaque enhancement would reflect inflammatory activity and that therefore the proposed imaging method would be a valuable tool for detecting plaque inflammation (21). The purpose of this study was to investigate the contributing factors for plaque enhancement and to investigate the relationship between regional contrast enhancement and inflammatory activity of atherosclerotic plaques in the experimental rabbit model by using contrast-enhanced high-resolution 3D black-blood MRI in comparison with histopathologic examination.

METHODS

Animal protocol. Ten male New Zealand white rabbits (weight 3.0 to 3.5 kg) were used for the animal model of atherosclerosis. Three male rabbits (weight 3.0 to 3.5 kg) were used as control animals and were maintained on a normal rabbit chow diet for 2 weeks. In the experimental rabbits, aortic atherosclerosis was induced by a combination of a high-cholesterol diet (0.3% cholesterol-enriched diet; Feedlab, Hanam, Korea) for 6 months and aortic balloon denudation injury performed twice (at 1 week and 1 month after starting the high-cholesterol diet).

After exposure of the iliac artery, a 4-F Fogarty embolectomy catheter was advanced through the aorta just above the diaphragm level. Then, the catheter balloon was inflated using a total of 0.5 ml of the diluted contrast agent. The aortic denudation injury was performed 3 times from the diaphragm to the iliac bifurcation (abdominal aorta). All procedures were performed under general anesthesia using tiletamine (30 mg/kg; Zoletil, Virbac, Carros, France) and xylazine (10 mg/kg; Rompun, Bayer, Hanam, Korea). The study protocol was approved by our Animal Care and Use Committee.

MRI. Under general anesthesia (tiletamine [20 mg/kg; Zoletil], Virbac, and xylazine [5 mg/kg; Rompun], Bayer), the rabbits were imaged in the craniocaudal direction and in the supine position in a 3.0-T whole-body magnetic resonance (MR) scanner (MAGNETOM Trio; Siemens Medical Solutions, Erlangen, Germany) using an 8-channel body coil. Three orthogonal localizer images confirmed the appropriate position of the rabbits. Thereafter,

high-resolution images were obtained using the proposed T1-weighted single-slab 3D black-blood turbo/fast spin-echo pulse sequence with fat suppression before and after the administration of contrast agents (21). To reduce signal modulations in k-space and to alleviate image blurring, variable flip angles were used in the refocusing pulse train. Blood signals were suppressed selectively by the following, flow-sensitizing schemes: 1) variable refocusing flip angles to increase the incoherence of blood signals; 2) motion-sensitizing gradient schemes in the readout direction; and 3) matching velocity encoding gradients on either side of the first refocusing pulse. Imaging parameters were as follows: repetition time/echo time, 630/24 ms; field of view, 192 × 128 mm^2; matrix, 320 × 214; echo train length, 17; signal averages, 4; slab thickness, 28.8 mm; number of z phase encodes, 48; integrated parallel acquisition technique (iPAT) factor, 2; and iPAT additional reference lines, 20. The scan range included the segment of the abdominal aorta immediately below the diaphragm to the iliac bifurcation. Two minutes after administration of 0.1 mmol/kg of gadolinium-based contrast agent (Gadodiamide; Omniscan, 0.5 mmol/ml, GE Healthcare, Cork, Ireland) via the ear vein, coronal T1-weighted imaging was repeated with the same protocol as the pre-contrast scan, which typically took 15 min.

Histopathologic analysis. Aortas were excised after a 4% phosphate-buffered paraformaldehyde (in phosphate-buffered saline) perfusion-fixation. Adventitia of the excised aorta was marked immediately with India ink at the posterior face of the artery to facilitate matching of the histologic slides and MRI scans. Serial sections of the abdominal aorta were cut at 3-mm intervals to match the corresponding MRI scans. Specimens were embedded in paraffin. Five-micrometer sections were cut and stained with Masson's trichrome and Van Gieson's stain. Additionally, all sections were stained immunohistochemically with RAM-11 antibody, which binds to macrophages (Dako, Carpinteria, California) and a CD-31 antibody, which binds to endothelial cells (clone JC70A, Dako). Aortic plaques were defined as structures thicker than 1 mm within or adjacent to the aortic lumen, or both, that could be distinguished clearly from the vessel lumen and the surrounding tissue.

Comparison of MRI results and histopathologic slices. The slices for each rabbit were numbered in a craniocaudal fashion to match image slices in the 2 methods (histopathologic and MRI examination). Because the thickness of the histologic section was 3 mm, 3D volumetric MR scans acquired with 0.6-mm resolution in the section direction were projected to reconstruct a 3-mm section using multiplanar reformatting post-processing software for comparison. For quantitative plaque analysis, 2 to 3 consecutive 3-mm slices located above and including the celiac artery, 2 to 3 consecutive 3-mm slices below the celiac trunk and including the superior mesenteric artery, and 5 consecutive 3-mm slices located below and including the left renal artery were selected and analyzed with the matching MRI scans and histopathologic images. After matching the MRI slices with the corresponding histopathologic slices, we compared every first slice of the histopathologic slices (5-μm thick section) with the original MRI slices (0.6 mm).

Image analysis of histopathologic results. We evaluated a total of 105 histopathologic sections for atherosclerotic wall and 28 histopathologic sections for the normal control. Of the atherosclerotic wall sections, we selected vessel walls thicker than 1 mm based on histopathologic examination for analysis. Forty-three of 105 histopathologic sections for atherosclerotic wall were excluded because of vessel walls thinner than 1 mm.

Ultimately, 62 histopathologic sections for atherosclerotic wall and 28 sections for the normal control were included in this study, and histopathologic sections and the matched MR scans were divided into 4 quadrants (atherosclerotic wall, n = 248, and normal wall, n = 72, respectively) for analysis (Fig. 1).

Histopathologic sections were digitized to the same computer. An independent pathologist, blinded to the results of the MRI, performed the histopathologic analysis. On histopathologic sections, lipid-rich areas were measured manually by drawing a loose matrix area where lipid-laden macrophages were abundant on sections stained with hematoxylin and eosin. Fibrous areas were measured manually by drawing the dense pinkish area on sections stained with hematoxylin and eosin, which corresponds to blue area stained with Masson's trichrome. Calcified areas were measured manually by drawing in the empty space within the plaques that contain remaining remnant spotty crystal deposit stained violet on hematoxylin and eosin and Van Gieson's stain. Areas were expressed in square millimeters for each quadrant. On histologic analysis, a plaque was considered to be lipid rich if the percentage of lipid-rich area was >50% of the total plaque area. Fibrous plaques were

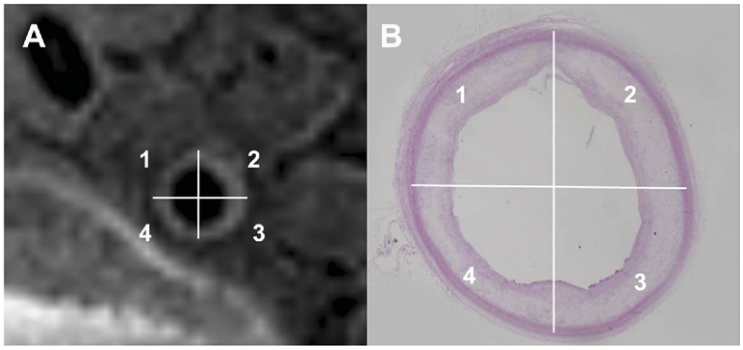

Figure 1. Transverse Pre-contrast MR Scan and Matched Photomicrograph of Hematoxylin and Eosin-Stained Section

(A) Transverse pre-contrast magnetic resonance imaging (MRI) scan with **(B)** matched histopathologic hematoxylin and eosin-stained section divided into 4 quadrants. Enhancement ratio (ER) values were evaluated in each quadrant. The ER of the signal intensity (SI) was calculated as follows: ER = SI_{post} /SI_{pre}, where SI_{post} is the SI of the wall after contrast enhancement and SI_{pre} is SI of the wall before contrast enhancement.

defined as having >50% of fibrous area of the total plaque area. Mixed plaques were defined as having >10% of calcified area of the total plaque area. There were only 5 mixed plaques based on histopathologic analysis. Macrophage content was measured manually by drawing in the brown area on sections stained with a RAM-11 antibody. The total macrophage area was normalized by dividing the total plaque area and was expressed as percentages for each quadrant. We defined a macrophage-rich plaque as having more than 50% of macrophage-stained area of the total plaque area.

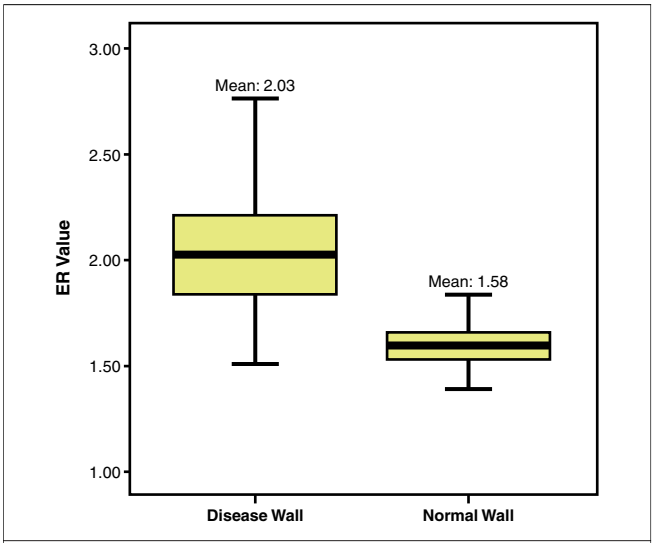

Figure 2. Box-and-Whisker Graph Showing ER Values for the Atherosclerotic Wall and the Normal Wall Determined by Histopathologic Analysis

The **lower and upper ends of the box** represent the 25th and 75th percentiles, respectively, and **a line across the box** indicates the median. The **whiskers** range from the fifth to 95th percentile. Abbreviation as in Figure 1.

Microvessel density was calculated by measuring the total number of microvessels in atherosclerotic plaques and dividing by total plaque area for each quadrant. All measurements of histologic analysis were performed using a computer-assisted quantitative color image analysis system (Image Pro-Plus, Media Cybernetics, Inc., Bethesda, Maryland) for each slice.

Image analysis of MR results. The MR scans were transferred to a dedicated workstation (Aquarius, TeraRecon, Inc., San Mateo, California) for analysis. On MR scans, aortic plaques are defined as structures of thickened aortic wall thicker than 1 mm that can be distinguished clearly from the vessel lumen and the surrounding tissue.

After matching the MR scan with the corresponding histopathologic slices, wall and lumen signal intensities (SIs) were determined with standard region-of-interest measurements. To obtain plaque SI values, regions of interest were manually placed inside the matched plaques. Two radiologists (J.H., B.W.C.) independently measured the SI at 3 randomly selected points for each quadrant. The mean SI values measured by 2 radiologists were used for analysis. Enhancement ratio (ER) of the SI was calculated as follows; ER = SI_{post}/SI_{pre}, where SI_{post} is the SI of the wall after contrast enhancement and SI_{pre} is SI of the wall before contrast enhancement.

Statistical analysis. Statistical significance of differences in calculated ER of aortic walls between atherosclerotic rabbits and normal controls was assessed using a Student *t* test for independent samples. The statistical significance of differences in calculated ER of plaques according to different

Table 1. Enhancement Ratio Measurements of Lipid-Rich and Fibrous Quadrants

	SI_{pre}	SI_{post}	ER*
Lipid-rich quadrants	238 ± 41 (168 to 331)	509 ± 117 (285 to 707)	2.14 ± 0.31 (1.33 to 2.81)
Fibrous quadrants	231 ± 39 (165 to 314)	425 ± 95 (267 to 654)	1.84 ± 0.21 (1.24 to 2.51)

Values are mean ± SD (range). *Calculated as: ER = SI_{post}/SI_{pre}. ER = enhancement ratio; SI = signal intensity; SI_{pre} = signal intensity of the wall before contrast enhancement; SI_{post} = signal intensity of the wall after contrast enhancement.

plaque types determined by histopathologic analysis was assessed using a Student *t* test for independent samples. Correlations between ER of the plaques and the histologic variables, including the percentage of macrophage areas and the microvessel density, were performed using Pearson correlation coefficient. Multiple linear regression analysis was performed to determine independent factors for plaque enhancement. In addition, Pearson correlation was used to determine the correlation of mean values between the 2 observers. Values of $p < 0.05$ were considered statistically significant. SPSS software version 10.0 (SPSS, Inc., Chicago, Illinois) was used for statistical analysis.

RESULTS

A total of 62 plaques, including 57 noncalcified plaques and 5 mixed plaques (n = 248: 156 lipid-rich quadrants and 92 fibrous quadrants) were identified based on histopathologic analysis. On plaque-based analysis, the mean ER values were found to be significantly different with 1.58 ± 0.15 and 2.03 ± 0.25 values for normal and atherosclerotic aortic walls, respectively (p = 0.017) (Fig. 2).

The mean ER values for each quadrant are summarized in Table 1. The mean ER values were 2.14 ± 0.31 and 1.84 ± 0.21 for the lipid-rich and fibrous quadrants, respectively. The mean ER values were significantly different between the lipid-rich quadrants and fibrous quadrants (p = 0.001).

When each quadrant was divided into 2 groups according to the percentage of macrophage area using a cutoff value of 50%, the ER values were significantly different between the macrophage-rich plaques and the macrophage-poor plaques (n = 136, 2.21 ± 0.28 vs. n = 112, 1.81 ± 0.22; p = 0.001) (Figs. 3 and 4). The mean ER values showed moderate correlations with the percentage of macrophage area (r = 0.645; p < 0.001) (Fig. 5). In addition, microvessel density was found to be significantly different with 119.3 ± 43.8 and 76.9 ± 35.4 values for macrophage-rich and macrophage-poor plaques (p = 0.001). The mean ER values showed moderate correlation with the microvessel density (r = 0.598; p < 0.001) (Fig. 6).

The percentage of macrophage area was 51 ± 19% for the lipid-rich quadrant and 35 ± 17% for the fibrous quadrants. The percentage of macrophage area was significantly different between the lipid-rich quadrants and fibrous quadrants (p = 0.001). The microvessel density was 112.4 ± 45.2 for the lipid-rich quadrant and 79.4 ± 35.7 for the fibrous quadrants. The microvessel density was significantly different between the lipid-rich quadrants and fibrous quadrants (p = 0.005).

To discover factors that contributed to plaque enhancement, we used a multivariate linear regression model in which ER values were the dependent variable, and total plaque area, including components and histologic variables, were entered as independent predictors. On multiple regression analysis, the percentage of macrophage area and microvessel density were associated independently with ER values, which represented plaque enhancement (p < 0.001) (Table 2). There was good

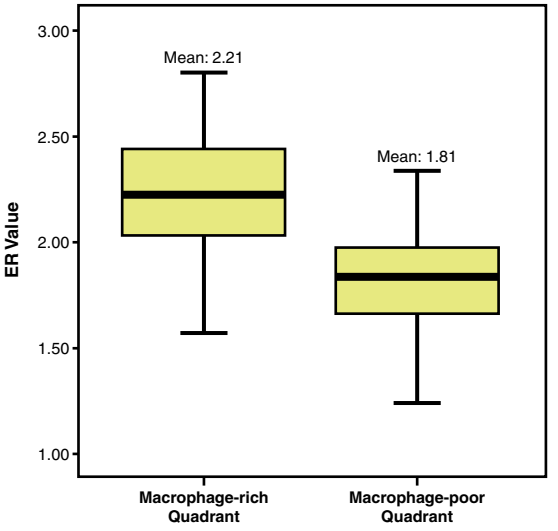

Figure 3. Box-and-Whisker Graph Showing ER Values for the Macrophage-Rich Plaques and the Macrophage-Poor Plaques Determined by Histopathologic Analysis

The **lower and upper ends of the box** represent the 25th and 75th percentiles, respectively, and **a line across the box** indicates the median. The **whiskers** range from the fifth to 95th percentile. A plaque was considered macrophage-rich if the percentage of macrophage area was more than 50% of the total plaque area. Abbreviation as in Figure 1.

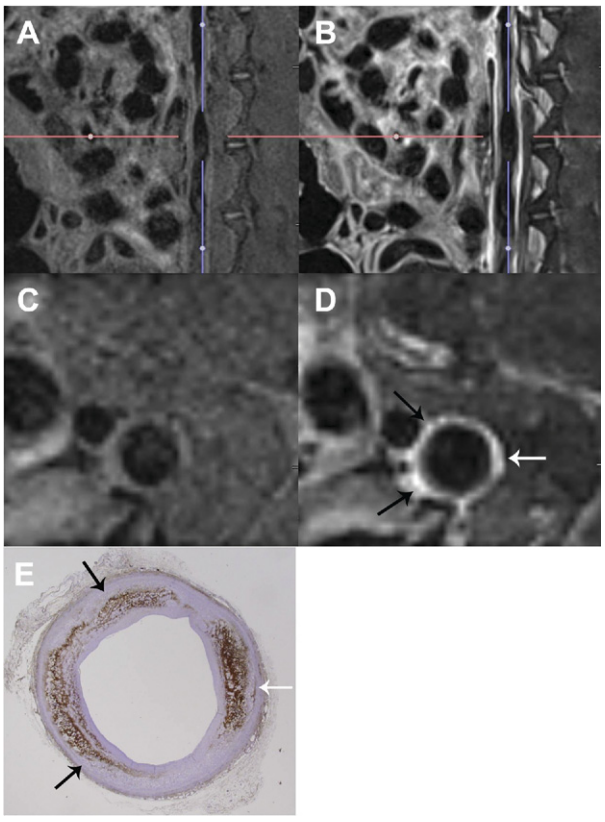

Figure 4. MR Scans and Corresponding Transverse Slices at the Level of the Cross Hairs

(A and **C)** Three-dimensional high-resolution pre–T1-weighted MR scan and corresponding transverse slice at the level of the cross hairs. **(B and D)** Three-dimensional high-resolution post–T1-weighted MRI scan and corresponding transverse slice at the level of the cross hairs. On post-contrast transverse MRI scan **(D)**, the atherosclerotic wall showed marked contrast enhancement **(white and black arrows)**. **(E)** Corresponding histopathologic section (RAM-11–positive staining; magnification, ×12.5) demonstrates abundant macrophage accumulation **(white and black arrows)** in the area matched with marked contrast enhanced area on MR scan. Abbreviation as in Figure 1.

interobserver agreement for the ER values for the lipid-rich and fibrous quadrants (r = 0.775 and r = 0.768, respectively).

DISCUSSION

It recently was shown that inflammation plays a critical role in plaque initiation, progression, and disruption and represents an emerging target for the treatment of atherosclerosis (7,8). For this underlying mechanism, neovessels are known to play a key role in the progression of atherosclerotic plaques by providing routes of leukocyte recruitment into the plaque region. Several studies reported a higher neovessel count in highly inflamed macrophage-rich atherosclerotic plaques compared with fibrocalcific lesions (9,14). These findings suggested that macrophage-rich atherosclerotic plaques, which were active inflammatory plaques, could be enhanced relative to macrophage-poor atherosclerotic plaques. Strong evidence suggests that plaques with high macrophage accumulation within the plaque and significant neovascularization are unstable and susceptible to rupture (7–10). Therefore, the ability to assess quantitatively the inflammatory status of a plaque using noninvasive imaging could be of tremendous value for studies evaluating the effectiveness of novel therapies intended to inhibit plaque inflammation.

MRI is a leading candidate for staging plaque stability because of its ability to image the vessel wall directly at high resolution. In particular, contrast-enhanced MRI using extracellular gadolinium-based contrast agents has shown promise for highlighting specific plaque components, allowing determination of the thickness of the fibrous cap, plaque composition, and the degree of plaque inflammation and neovascularization. Several studies have reported that patchy contrast enhancement in advanced plaques may be indicative of increased inflammatory activity (11,12). However, the underlying mechanism of plaque enhancement is likely to be multifactorial and has not been elucidated fully (12). Gadolinium-based contrast agents are known to distribute passively from the intravascular into the extracellular fluid space. This enhancement may be the result of increased permeability, increased extracellular volume, decreased washout of the contrast agent, or a combination thereof (12). Therefore, loose matrix, inflammation, and neovasculature were associated with stronger enhancement with the use of gadolinium-based contrast agents in atherosclerotic plaque. Several studies have reported that gadolinium-based contrast agents are not specific and therefore are inadequate for plaque imaging (15–17). Lobbes et al. (15) reported that Gd-DTPA was not able to discriminate between normal and atherosclerotic vessel walls. Barkhausen et al. (16) reported the inability to distinguish between Watanabe rabbit wall segments with and without plaque burden directly after administration of Gd-DTPA. In this study, ER values were shown to be significantly higher in atherosclerotic vessel walls compared with controls, which may be explained by the use of a different analysis method and different MRI protocol. In our study, we divided the atherosclerotic wall into 4 quadrants and evaluated each quadrant because of difficulty in correctly quantifying ER values using single representative values for diffuse atherosclerotic walls. However, in previous studies, plaque enhancement

was analyzed for each section. Additionally, we used a newly developed 3D high-resolution MRI for plaque imaging, instead of the 2D MRI sequences used by Barkhausen et al. (16). Reliable detection and reproducible measurements of plaque components or enhancement using 2D MRI are difficult to obtain because of the partial volume effect, and gross morphological measurements in serial studies are prone to errors caused by variation in slice position and alignment. Three-dimensional high-resolution imaging can provide increased resolution in the slice-select direction with an increased signal-to-noise ratio, and therefore may be more advantageous to use than 2D MRI. Another possible explanation could be that we included aortic plaques thicker than 1 mm, which raises the interesting possibility that the link between enhancement and inflammation only arises in more advanced plaques.

Previous studies with contrast-enhanced MRI have shown that the fibrous cap in atherosclerotic carotid plaques is enhanced with gadolinium-based contrast agents. Conversely, the lipid-rich necrotic core, which lacks vasculature and matrix, shows slight to no enhancement (11,12). Yuan et al. (11) showed that the enhancement of fibrous tissue was moderate to strong (79.5 ± 29.1%), whereas the lipid-rich necrotic core was enhanced only slightly (28.8 ± 20.1%). The differences between enhancement of fibrous tissue and lipid-rich necrotic core were significant. In our study, lipid-rich plaques exhibited significantly stronger plaque enhancement than fibrous plaques. This was because of the different pathologic features between the rabbit atherosclerotic plaque and human carotid plaque. The lipid-rich areas in rabbit atherosclerotic plaques generally do not contain necrotic cores. Rather, they are accumulations of living, macrophage-derived foam cells. Another possible explanation could be that we performed post–contrast-enhanced MR scanning 2 min after Gd-DTPA administration, which is a relatively early phase procedure compared with a delayed enhanced MRI protocol. It is known from delayed enhanced cardiac MRI, which is usually acquired 10 to 15 min after administration of contrast material, that contrast enhancement also can be the result of fibrosis, and to date, delayed enhanced cardiac MRI has been used to evaluate myocardial fibrosis in various cardiac diseases (22,23). This finding suggests that macrophage accumulation is more important for plaque enhancement than fibrous tissue for early contrast enhancement.

Recently, dynamic contrast-enhanced (DCE) MRI has been applied to the study of atherosclerotic plaques in human patients using a bright-blood DCE technique. Kerwin et al. (9,10) reported that a contrast agent uptake parameter such as K_{trans} on DCE MRI showed a positive linear correlation

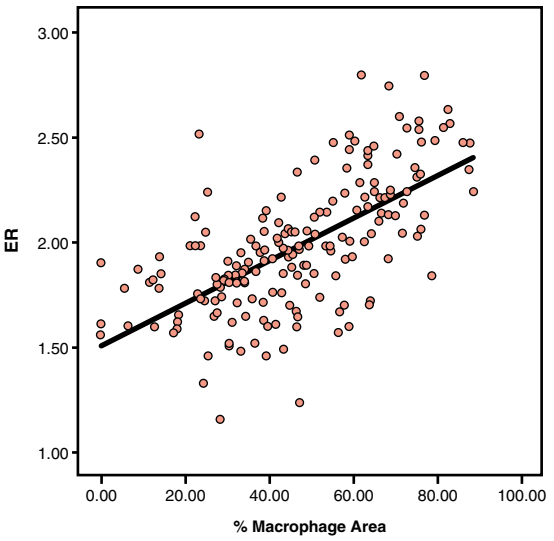

Figure 5. Scatterplot Showing ER Values Compared With the Percentage of Macrophage Area for the Atherosclerotic Plaques on Histopathologic Analysis With Regression Lines

The correlation coefficient was 0.645. ER = SI_{post}/SI_{pre}, where SI_{post} is the SI of the wall after contrast enhancement and SI_{pre} is SI of the wall before contrast enhancement. Abbreviations as in Figure 1.

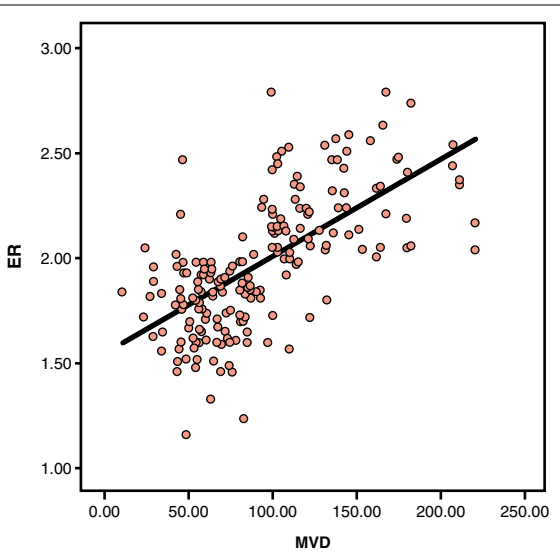

Figure 6. Scatterplot Showing ER Values Compared With the Microvessel Density for the Atherosclerotic Plaques on Histopathologic Analysis With Regression Lines

The correlation coefficient was 0.598. ER = SI_{post}/SI_{pre}, where SI_{post} is the SI of the wall after contrast enhancement and SI_{pre} is SI of the wall before contrast enhancement. MVD = microvessel density; other abbreviations as in Figure 1.

Table 2. Results of the Multiple Linear Regression Model

Parameters	ER (Adjusted R^2 = 0.437)		
	Unstandardized Coefficient (Standardized)	SE	p Value
Total plaque area	0.047 (0.111)	0.023	0.156
% of lipid area	–0.001 (–0.06)	0.005	0.522
% of fibrous area	–0.003 (–0.131)	0.005	0.418
% of macrophage area	0.009 (0.599)	0.001	<0.001
Microvessel density	0.006 (0.436)	0.001	<0.001

Abbreviation as in Table 1.

with neovessel density and macrophage count, which were histologic markers of plaque inflammation. However, the use of bright-blood techniques makes it intrinsically difficult to delineate the vessel wall and plaque for future analyses. In our study, we confirmed and quantified the signal enhancement of plaque after Gd-DTPA administration using ER values in atherosclerotic rabbit vessel walls. In this study, post–contrast-enhanced MR scanning 2 min after Gd-DTPA administration was performed based on a previous study by Calcagno et al. (14). They found strong contrast enhancement of atherosclerotic wall 2 min after Gd-DTPA administration and a significant positive correlation between the area under the signal intensity versus time curve calculated from DCE MRI at 2 and 7 min after injection and neovessel count. According to our study, macrophage accumulation and microvessel density were independent contributing factors for plaque enhancement. Therefore, we believe that ER values can be used to predict inflammatory activity within the plaque, which is a much simpler parameter for analysis.

Study limitations. There are some limitations to this study. First, histopathologic examination was used as the standard for MRI assessment. However, the processing of samples for examination by histopathologic analysis results in the shrinkage of the specimen and makes a comparison of absolute values difficult. In addition, some variability arises because of differences in slice thickness in the z direction on MRI and histologic examination. Second, abdominal aortic lesions were induced in a well-established rabbit model for atherosclerosis (24). However, the size and composition of atherosclerotic plaques in this experimental rabbit model are different from complex atherosclerotic plaques in humans. Human atheroma, in contrast to the rabbit model, progresses toward plaque vulnerability and rupture, which is important in the clinical situations (25,26).

CONCLUSIONS

Our results show that the percentage of macrophage area and microvessel density was associated independently with plaque enhancement, reflecting the occurrence of plaque inflammation. Based on these results, we believe that contrast-enhanced high-resolution 3D black-blood MRI may be an efficient way to detect plaque inflammation. In addition, the ability to assess quantitatively the inflammatory status of a plaque using high-resolution 3D black-blood MRI will be of tremendous value for monitoring the therapeutic effect intended to inhibit plaque inflammation in the future.

Acknowledgment

The authors thank Nam Hee Park for technical assistance.

Reprint requests and correspondence: Dr. Byoung Wook Choi, Department of Radiology, Severance Hospital, Yonsei University College of Medicine, 250 Seongsanno (134 Sinchon-dong), Seodaemun-gu, Seoul 120-752, South Korea. *E-mail: bchoi@yuhs.ac.*

REFERENCES

1. Carr S, Farb A, Pearce WH, Virmani R, Yao JS. Atherosclerotic plaque rupture in symptomatic carotid artery stenosis. J Vasc Surg 1996;23:755–65, discussion 765–6.
2. Virmani R, Burke AP, Kolodgie FD, Farb A. Vulnerable plaque: the pathology of unstable coronary lesions. J Interv Cardiol 2002;15:439–46.
3. Virmani R, Burke AP, Farb A, Kolodgie FD. Pathology of the vulnerable plaque. J Am Coll Cardiol 2006;47:C13–8.
4. Fuster V, Moreno PR, Fayad ZA, Corti R, Badimon JJ. Atherothrombosis and high-risk plaque. Part I: evolving concepts. J Am Coll Cardiol 2005;46:937–54.
5. Libby P. Current concepts of the pathogenesis of the acute coronary syndromes. Circulation 2001;104:365–72.
6. Kolodgie FD, Burke AP, Farb A, et al. The thin-cap fibroatheroma: a type of vulnerable plaque: the major precursor lesion to acute coronary syndromes. Curr Opin Cardiol 2001;16:285–92.
7. Saam T, Hatsukami TS, Takaya N, et al. The vulnerable, or high-risk, atherosclerotic plaque: noninvasive MR imaging for characterization and assessment. Radiology 2007;244:64–77.
8. Hansson GK. Inflammation, atherosclerosis, and coronary artery disease. N Engl J Med 2005;352:1685–95.
9. Kerwin W, Hooker A, Spilker M, et al. Quantitative magnetic resonance imaging analysis of neovasculature volume in carotid atherosclerotic plaque. Circulation 2003;107:851–6.

10. Kerwin WS, O'Brien KD, Ferguson MS, Polissar N, Hatsukami TS, Yuan C. Inflammation in carotid atherosclerotic plaque: a dynamic contrast-enhanced MR imaging study. Radiology 2006;241:459–68.
11. Yuan C, Kerwin WS, Ferguson MS, et al. Contrast-enhanced high resolution MRI for atherosclerotic carotid artery tissue characterization. J Magn Reson Imaging 2002;15:52–67.
12. Wasserman BA, Smith WI, Trout HH, Cannon RO, Balaban RS, Arai AE. Carotid artery atherosclerosis: in vivo morphologic characterization with gadolinium enhanced double-oblique MR imaging—initial results. Radiology 2002;223:566–73.
13. Cai J, Hatsukami TS, Ferguson MS, et al. In vivo quantitative measurement of intact fibrous cap and lipid-rich necrotic core size in atherosclerotic carotid plaque; comparison of high-resolution, contrast-enhanced magnetic resonance imaging and histology. Circulation 2005;112: 3437–44.
14. Calcagno C, Cornily JC, Hyafil F, et al. Detection of neovessels in atherosclerotic plaques of rabbits using dynamic contrast enhanced MRI and 18F-FDG PET. Arterioscler Thromb Vasc Biol 2008;28:1311–7.
15. Lobbes MB, Miserus RJ, Heeneman S, et al. Atherosclerosis: contrast-enhanced MR imaging of vessel wall in rabbit model-comparison of gadofosveset and gadopentetate dimeglumine. Radiology 2009;250:682–91.
16. Barkhausen J, Ebert W, Heyer C, Debatin JF, Weinmann HJ. Detection of atherosclerotic plaque with gadofluorine-enhanced magnetic resonance imaging. Circulation 2003; 108:605–9.
17. Ronald JA, Chen Y, Beliscle AJ, et al. Comparison of gadofluorine-M and Gd-DTPA for noninvasive staging of atherosclerotic plaque stability using MRI. Circ Cardiovasc Imaging 2009; 2:226–34.
18. Balu N, Chu B, Hatsukami Ts, Yuan C, Yarnykh VL. Comparison between 2D and 3D high-resolution black-blood techniques for carotid artery wall imaging in clinically significant atherosclerosis. J Magn Reson Imaging 2008;27:918–24.
19. Koktzoglou I, Chung YC, Carroll TJ, Simonetti OP, Morasch MD, Li D. Three-dimensional black-blood MR imaging of carotid arteries with segmented steady-state free precession: initial experience. Radiology 2007; 243:220–8.
20. Koktzoglou I, Li D. Diffusion-prepared segmented steady-state free precession: application to 3D black-blood cardiovascular magnetic resonance of the thoracic aorta and carotid artery walls. J Cardiovasc Magn Reson 2007;9:33–42.
21. Park J, Kim EY. Contrast-enhanced three-dimensional whole-brain black-blood imaging for efficient detection of small metastases. Magn Reson Med 2010;63:553–61.
22. Oshinski JN, Yang Z, Jones JR, Mata JF, French BA. Imaging time after Gd-DTPA injection is critical in using delayed enhancement to determine infarct size accurately with magnetic resonance imaging. Circulation 2001;104:2838–42.
23. Mahrholdt H, Wagner A, Judd RM, Sechtem U, Kim RJ. Delayed enhancement cardiovascular magnetic resonance assessment of non-ischaemic cardiomyopathies. Eur Heart J 2005;26:1461–74.
24. Viles-Gonzalez JF, Poon M, Sanz J, et al. In vivo 16-slice, multidetector row computed tomography for the assessment of experimental atherosclerosis: comparison with magnetic resonance imaging and histopathology. Circulation 2004;110:1467–72.
25. McMahon AC, Kritharides L, Lowe HC. Animal models of atherosclerosis progression: current concepts. Curr Drug Targets Cardiovasc Haematol Disord 2005;5:433–40.
26. Bengel FM. Atherosclerosis imaging on the molecular level. J Nucl Cardiol 2006;13:111–8.

Key Words: atherosclerosis ■ inflammation ■ magnetic resonance imaging ■ plaque.